CHINESE OPTICS LETTERS

Vol. 21, No. 9 | September 2023

Piezoelectric constant temperature dependence in strained [111]-oriented zinc-blende MQW-SOAs

Horacio Soto-Ortiz* and Gerson Torres-Miranda

Applied Physics Division, Center for Scientific Research and Higher Education of Ensenada, Ensenada 22860, Mexico

*Corresponding author: hsoto@cicese.mx

Received February 21, 2023 | Accepted May 31, 2023 | Posted Online August 22, 2023

Here, we present a study of the effective piezoelectric constant (e_{14_e}) temperature dependence in strained [111]-oriented zinc-blende quantum wells (QWs) embedded within a semiconductor optical amplifier (SOA). We determined e_{14_e} using a method that was insensitive to the segregation phenomenon and to the temperature dependence of the bandgap energy, which required neither fitting parameters nor temperature-dependent expressions for energy and out-of-plane effective masses of electrons and heavy holes. An $e_{14_e} = -0.0534 \pm 0.0040$ C · m^{-2} at 23°C was obtained for an SOA with 1.2 nm [111]-oriented strained $In_{0.687}Ga_{0.313}As/In_{0.807}Ga_{0.193}As_{0.304}P_{0.696}$ QWs. Unlike previously published research, where e_{14_e} magnitude increased as temperature rised, we extracted an e_{14_e} magnitude that decreased as temperature increased.

Keywords: piezoelectric constant; pyroelectric effect; quantum-confined Stark effect; excitons; semiconductor optical amplifiers; zinc-blende; quantum wells.

DOI: 10.3788/COL202321.092501

1. Introduction

Due to the abrupt changes in absorption and refractive index that the quantum-confined Stark effect (QCSE) can potentially induce in a low-dimensional structure, this mechanism has excellent potential for developing ultra-fast all-optical functions for telecommunications systems using strained [111]-oriented zinc-blende multiple quantum well semiconductor optical amplifiers (MQW-SOAs)[1,2]. Indeed, these amplifiers, compared to the massive ones, exhibit higher differential gains, lower noise figures, and, notably, an internal piezoelectric field that is mainly responsible for the QCSE when they are unbiased[3,4]. Therefore, to estimate the temperature dependence of the QCSE in MQW-SOAs and thus be able to use it as a contribution to tune the energy of the excitonic resonances where required for a specific application, it is crucial to determine the temperature dependence of the piezoelectric constant e_{14}. Some authors estimate e_{14} using linear interpolation between the piezoelectric constant values of the relevant binary semiconductors of the alloy of the quantum wells (QWs)[3,5]. Nevertheless, this procedure generates larger e_{14} values than those obtained experimentally. Concerning the piezoelectric constant experimental determination in QWs, typically, e_{14} is used as an adjustment parameter in theoretical models to fit the calculated values of the energies of determined electronic transitions affected by the QCSE, to those obtained experimentally[6]. e_{14} is also estimated by extracting key parameters from the Franz–Keldysh oscillations that allow its indirect determination[7]. However, in structures where, during the growth of the monolayers of the QW alloy, the surface segregation phenomenon can occur, the e_{14} experimental determination becomes complex since this phenomenon produces a blue shift of the fundamental transition energy[8–10]. Therefore, methods used for determining e_{14}, based on the calculations of the energy levels, should consider this effect, although it is rarely included in them and probably because it substantially increases their degree of difficulty. Furthermore, when these methods are used to calculate e_{14} as a function of temperature, they have the drawback that temperature also has a marked effect on the bandgap energy of the material constituting the QWs. Thus, as the temperature fluctuates, the energy of the electronic transitions or the extremes of the Franz–Keldysh oscillations is simultaneously affected by two remarkable effects: the temperature dependence that the bandgap energy presents and that exhibited by the piezoelectric constant. These simultaneous effects may generate erroneous e_{14} experimental results or, at best, complicate its experimental determination.

Here, we use a simple method for experimentally determining the effective piezoelectric constant e_{14_e}, as a function of temperature, in strained zinc-blende QWs grown along the [111] direction of SOAs with a p-iMQW-n diode structure. Because the surface segregation phenomenon can impose a profile of values on e_{14}, by effective piezoelectric constant, we mean the global magnitude that is assigned to e_{14}. The used method, based on

© 2023 Chinese Optics Letters

the determination of the relative Stark shifts that the QCSE induces in the fundamental excitonic resonance when the electrodes of the MQW-SOA under test are short- and open-circuited, is insensitive to the variation of the bandgap energy with temperature. Likewise, the method is insensitive to the bandgap energy shift that may cause the surface segregation phenomenon. Even though the method was used to determine e_{14_e} in an MQW-SOA, it can be applied to any p-iMQW-n diode structure with electrodes and strained identical zinc-blende QWs grown along the [111] direction. In particular, we estimated e_{14_e} in a temperature range of interest for telecommunication applications (18–28°C).

2. Methods

In strained zinc-blende QWs grown along the [111] direction of unbiased SOAs with a p-iMQW-n diode structure, the excitonic transition energy from the first electronic state to the first heavy-hole state (1s e-hh) can be represented as follows when the amplifier electrodes are short-circuited ($E_{x_{\mathrm{sc}}}$) or open-circuited ($E_{x_{\mathrm{oc}_n}}$):

$$E_{x_{\mathrm{sc,oc}_n}} = E_g(T, \delta E_{\mathrm{hy}}, \delta E_{\mathrm{sh}}, \phi_{x_i}) + E_q - E_b + \Delta E_{s_{\mathrm{sc,oc}_n}}(T, F_{w_n}), \tag{1}$$

where sub-subscript n indicates dependence on the input power, namely, on the used nth discrete value of the optical input power (P_{in_n}). E_g is the QW alloy bandgap energy, which is a function of temperature T, hydrostatic deformation energy δE_{hy}, shear deformation energy δE_{sh}, and chemical modulation ϕ_{x_i} that the QW alloy could undergo due to the surface segregation phenomenon. E_q is the ground state total quantization energy of the conduction and heavy-hole (hh) valence bands when QWs are unperturbed ($F_{w_n} = P_{\mathrm{in}_n} = 0$). E_b is the 1s e-hh exciton binding energy, and $\Delta E_{s_{\mathrm{sc,oc}_n}}$ is the total Stark shift of the 1s e-hh excitonic resonance ($1\mathrm{S}_{\text{e-hh}}\mathrm{ER}$) caused by the total electric field F_{w_n} acting on each of the QWs when the MQW-SOA electrodes are short-(SC) and open-circuited (OC).

In the present analysis, it was assumed the MQW-SOA structure under study is composed of identical QWs, and the F_{w_n} and piezoelectric fields are the same in all the wells. Based on these considerations, F_{w_n} can be given by[4]

$$F_{w_n}(T) \approx \frac{\varepsilon_i}{\varepsilon_w}\frac{V_{\mathrm{bt}_n}(T)}{L_i} - e_{14_e}(T)\frac{L_i - mL_w}{L_i}\eta_{xy}, \tag{2}$$

where ε_i and ε_w are the static dielectric constants of the intrinsic layer and the QW layers, respectively; L_i is the intrinsic region thickness; m is the number of QWs; L_w is the width of the QWs; ε_0 is the vacuum permittivity; $-\eta_{xy}e_{14_e}(T)$ is the piezoelectric field (F_{wp}) acting on each QW; and η_{xy} is the shear strain times $2\sqrt{3}(\varepsilon_w\varepsilon_0)^{-1}$ defined as

$$\eta_{xy} = \frac{2\sqrt{3}}{\varepsilon_w\varepsilon_0}\left(\frac{C_{11_w} + 2C_{12_w}}{C_{11_w} + 2C_{12_w} + 4C_{44_w}}\right)\varepsilon_s, \tag{3}$$

where ε_s is the lattice mismatch strain, and C_{11_w}, C_{12_w}, and C_{44_w} are the elastic stiffness coefficients of the material of the QWs, which can be estimated, as can ε_i and ε_w, by Vergard's Law[4]. Furthermore, in Eq. (2), $V_{\mathrm{bt}_n}(T)$ is the effective built-in potential drop across the p-i-n diode, which is a function of temperature, contact potential difference, piezoelectric fields in the QWs, and electric fields created by dipoles formed by photogenerated electron-hole pairs inside and outside the QWs (in-well and long-range screening fields). It is noteworthy that, at temperature T, $V_{\mathrm{bt}_n}(T)$ can be determined experimentally as a function of the optical power using a digital multimeter operating in the diode-test mode with its test leads connected between the MQW-SOA electrodes in such a way that it is forward-biased.

Considering that F_{w_n} causes a negligible change in E_b, from Eq. (1), the energy difference ($\Delta E_{x_{\mathrm{os}_n}} = E_{x_{\mathrm{oc}_n}} - E_{x_{\mathrm{sc}}}$) existing between the $1\mathrm{S}_{\text{e-hh}}\mathrm{ER}$ energies under open- and short- circuit conditions (OCC and SCC) becomes practically equal to the total Stark shift difference ($\Delta E_{s_{\mathrm{oc}_n}} - \Delta E_{s_{\mathrm{sc}}}$) experiencing $1\mathrm{S}_{\text{e-hh}}\mathrm{ER}$ under OCC and SCC[11]. Indeed, since the energies $E_{x_{\mathrm{oc}_n}}$ and $E_{x_{\mathrm{sc}}}$ are defined by Eq. (1), their difference, for the same temperature, causes the cancellation of E_g, E_q, and E_b, and therefore of the effects of temperature and segregation phenomenon on E_g. Consequently, $\Delta E_{x_{\mathrm{os}_n}}$ is given in eV by[11,12]

$$\begin{aligned}\Delta E_{x_{\mathrm{os}_n}} &= \Delta E_{s_{\mathrm{oc}_n}} - \Delta E_{s_{\mathrm{sc}}} \\ &= (-\bar{A}_{\mathrm{ehh}}L_w^4F_{w_n}^2 + Q_qL_{iws_n}F_{w_n}) - (-\bar{A}_{\mathrm{ehh}}L_w^4F_{w_{\mathrm{sc}}}^2),\end{aligned} \tag{4}$$

where $\bar{A}_{\mathrm{ehh}}$ is a function of the electron (heavy hole) out-of-plane effective mass in the QWs and the ground state energy shift enhancement factor, at low fields, due to the finite value of the barrier height for the electrons (heavy holes)[12]. Moreover, $F_{w_{\mathrm{sc}}}$ is the maximum value of F_{w_n}, which is obtained when the amplifier electrodes are short-circuited and thus $V_{\mathrm{bt}_n} = 0$ [see Eq. (2)], Q_q is the elementary charge times 6.2415×10^{18} eV/J and L_{iws_n} is the spatial separation, induced by F_{w_n} within the QWs, of the photogenerated electron and hole wave functions. For input powers that, under OCC, produce such a piezoelectric field screening that the $1\mathrm{S}_{\text{e-hh}}\mathrm{ER}$ energy undergoes a shift of less than 1.0 meV, it can be assumed F_{wp} is strong enough for F_{w_n} to induce a spatial separation between the photogenerated electron and hole wave functions close to the largest possible (L_w) [4]. Under these conditions, $L_{iws_n} \approx L_w$. Thus, substituting Eq. (2) into Eq. (4) and solving it for e_{14_e} results in the following expression:

$$e_{14_e} = \frac{\frac{\varepsilon_i}{\varepsilon_w}V_{\mathrm{bt}_1}(L_iL_wQ_q - \bar{A}_{\mathrm{ehh}}\frac{\varepsilon_i}{\varepsilon_w}L_w^4V_{\mathrm{bt}_1}) - \Delta E_{x_{\mathrm{os}_1}}L_i^2}{\eta_{xy}(L_i - mL_w)(L_iL_wQ_q - 2\bar{A}_{\mathrm{ehh}}\frac{\varepsilon_i}{\varepsilon_w}L_w^4V_{\mathrm{bt}_1})}. \tag{5}$$

Here, $\Delta E_{x_{\mathrm{os}_1}}$ and V_{bt_1} are the values that $\Delta E_{x_{\mathrm{os}_n}}$ and V_{bt_n} assume, respectively, when the input power is P_{in_1}. On the other hand, using two input powers, P_{in_1} and P_{in_2}, a system of two coupled equations can be obtained from Eq. (5), whose resolution results in the following expression for $\bar{A}_{\mathrm{ehh}}$:

$$\bar{A}_{\mathrm{ehh}} = \frac{[-2W_- + L_w Q_q (V_{\mathrm{bt}_1}^2 - V_{\mathrm{bt}_2}^2)\varepsilon_i/\varepsilon_w]L_i}{4V_{\mathrm{bt}_1}V_{\mathrm{bt}_2}L_w^4(V_{\mathrm{bt}_1} - V_{\mathrm{bt}_2})\varepsilon_i^2/\varepsilon_w^2} - \frac{L_i\sqrt{R - 4V_{\mathrm{bt}_1}V_{\mathrm{bt}_2}L_i^2\Delta E_{x_{\mathrm{os}_1}}\Delta E_{x_{\mathrm{os}_2}}}}{2V_{\mathrm{bt}_1}V_{\mathrm{bt}_2}L_w^4(V_{\mathrm{bt}_1} - V_{\mathrm{bt}_2})\varepsilon_i^2/\varepsilon_w^2}, \quad (6)$$

being

$$R = W_+^2 + L_w Q (V_{\mathrm{bt}_1} - V_{\mathrm{bt}_2})^2 (W_+ + M)\varepsilon_i/\varepsilon_w, \quad (7)$$

$$W_\pm = L_i(\Delta E_{x_{\mathrm{os}_1}} V_{\mathrm{bt}_2} \pm \Delta E_{x_{\mathrm{os}_2}} V_{\mathrm{bt}_1}), \quad (8)$$

$$M = \left[\frac{1}{4}(V_{\mathrm{bt}_1} - V_{\mathrm{bt}_2})^2 - V_{\mathrm{bt}_1}V_{\mathrm{bt}_2}\right] L_w Q_q \varepsilon_i/\varepsilon_w, \quad (9)$$

where $\Delta E_{x_{\mathrm{os}_2}}$ and V_{bt_2} are the values that $\Delta E_{x_{\mathrm{os}_n}}$ and V_{bt_n} adopt, respectively, when the input power is P_{in_2}.

For notation simplicity, in Eqs. (5)–(9), the temperature dependence of e_{14_e}, $\bar{A}_{\mathrm{ehh}}$, $V_{\mathrm{bt}_{1,2}}$, $\Delta E_{x_{\mathrm{os}_{1,2}}}$, $W_\pm$, M, and R is omitted.

According to what is established above, by substituting Eq. (3) and Eqs. (6)–(9) into Eq. (5), and measuring $V_{\mathrm{bt}_{1,2}}$ and $\Delta E_{x_{\mathrm{os}_{1,2}}}$ for different temperatures, it is possible to determine $e_{14_e}(T)$.

3. Results and Discussion

Now, we use the procedure explained above for estimating the e_{14_e} value within the [111]-oriented strained $In_{0.687}Ga_{0.313}As/In_{0.807}Ga_{0.193}As_{0.304}P_{0.696}$ QWs of an unbiased MQW-SOA. The amplifier comprises a p-iMQW-n structure with a 2.2-μm-wide and 0.1-μm-thick intrinsic active region incorporating a central section, with eight QWs separated by seven barriers clad on both sides by a 28.4-nm-thick undoped $In_{0.807}Ga_{0.193}As_{0.304}P_{0.696}$ separate-confinement heterostructure (SCH). The QW and barrier widths are nominally 1.2 nm and 4.8 nm, respectively, and the QWs are subjected to a compressive lattice mismatch strain of $\varepsilon_s = -0.0142$. Moreover, $\varepsilon_i/\varepsilon_w = 0.904$ and $\varepsilon_w = 14.122$.

First, we determine $\Delta E_{x_{\mathrm{os}_{1,2}}} = E_{x_{\mathrm{oc}_{1,2}}} - E_{x_{\mathrm{sc}}}$ when the total input power is $P_{\mathrm{in}_{1,2}}$ in the temperature range from 18 to 28°C. For this purpose, we use the setup shown in Fig. 1. where a probe beam and a control beam, whose photon energy (1569 nm) is located well within the continuum spectrum, are launched in co-propagation into the amplifier with horizontal linear polarization. At a specific temperature within the range from 18 to 28°C, the probe beam wavelength is swept across the $1S_{e\text{-}hh}$ER spectral width, keeping its input power constant at −15.9 dBm. For each examined wavelength and each total input power, defined as the sum of the input powers of the control and probe beams, the probe beam power at the amplifier output is determined, under SCC and OCC (using switch S1 in Fig. 1), via an optical spectrum analyzer (OSA) with a wavelength accuracy of $\Delta\lambda_{\mathrm{OSA}} = \pm 0.02$ nm (see Fig. 1). Figure 2 shows the obtained transmission spectra, around $1S_{e\text{-}hh}$ER, for

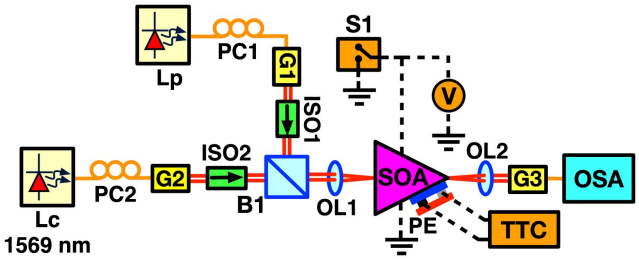

Fig. 1. Experimental setup. Solid, dashed, and double solid lines: optical fibers, electrical links, and free-space optical links. Lp and Lc, tunable laser; PC1 and PC2, polarization controller; G1, G2, G3, pigtailed graded-index lens collimator; ISO1 and ISO2, Faraday isolator; B1, beam splitter; OL1 and OL2, objective lens; SOA, MQW-SOA; OSA, optical spectrum analyzer; PE, Peltier element; S1, electric switch; V, digital multimeter; TTC, thermoelectric temperature controller.

the probe beam when the total input powers are $P_{\mathrm{in}_1} = -15.9$ dBm and $P_{\mathrm{in}_2} = -4.53$ dBm, and the amplifier temperatures are set at 18, 23, and 28°C under OCC. For the same temperatures but under SCC, Fig. 2 shows only transmission spectra obtained with a total input power of −15.9 dBm since these are identical to those acquired with a total input power of −4.53 dBm. Effectively, under steady-state and SCC, $V_{\mathrm{bt}_n} = 0$ and F_{w_n} becomes input power independent because the photogenerated carriers quickly escape from the QWs and are immediately drained by the MQW-SOA electrodes. Consequently, there are no free carriers inside or outside the QWs that can establish piezoelectric field screening mechanisms modifying the QCSE[4].

Figure 2 clearly shows how, with rising temperature, the $1S_{e\text{-}hh}$ER energy (indicated by arrows) red shifts. This is because $|e_{14_e}|$ decreases with temperature, causing $|F_{w_n}|$ to increase [see

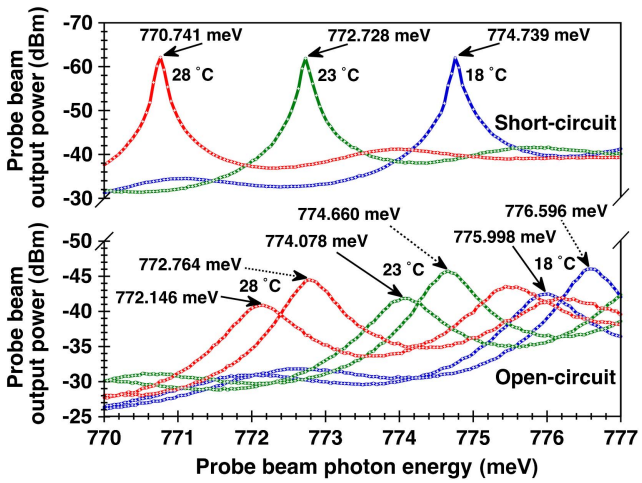

Fig. 2. Transmission spectra for $P_{\mathrm{in1}} = -15.9$ dBm and $P_{\mathrm{in2}} = -4.53$ dBm (indicated with solid and dashed arrows, respectively) at 18, 23, and 28°C under SCC (upper spectra) and OCC (lower spectra). Marks and traces are the measured values and their interpolations.

Eq. (2)]. Therefore, the deformation of the QWs is enhanced, resulting in a decrease in the carrier quantization energy. In particular, under SCC, the $1S_{e\text{-}hh}ER$ spectral position is shifted from 774.739 to 770.741 meV when the MQW-SOA temperature changes from 18 to 28°C, which corresponds to a tuning span of 4 meV (8.3 nm). From this figure, $\Delta E_{x_{os_{1,2}}} = E_{x_{oc_{1,2}}} - E_{x_{sc}}$, at 23°C, turns out to be approximately equal to $\Delta E_{x_{os_1}} = 774.078 - 772.728 = 1.35$ meV for P_{in_1}, and $\Delta E_{x_{os_2}} = 774.660 - 772.728 = 1.932$ meV for P_{in_2}. On the other hand, with the probe beam photon energy matching the $1S_{e\text{-}hh}ER$ central energy, the voltages $V_{bt_1} = 0.570$ V and $V_{bt_2} = 0.602$ V are measured with an accuracy of $\Delta V_{mul} = \pm 111\,\mu V$, under OCC, using a 6.5 digit multimeter in diode test mode (denoted as V in Fig. 1) for P_{in_1} and P_{in_2}, respectively.

Now, using Eqs. (3) and (5)–(9), as well as the found values for $\Delta E_{x_{os_{1,2}}}$ and $V_{bt_{1,2}}$, e_{14_e} at 23°C can be determined. Similarly, e_{14_e} can be estimated for any temperature. For clarity, Fig. 2 only shows the transmission spectra for 18, 23, and 28°C. However, the experimental determination of the $1S_{e\text{-}hh}ER$ energy under SCC ($E_{x_{sc}}$) and OCC ($E_{x_{oc_{1,2}}}$) and the voltages $V_{bt_{1,2}}$ was performed for eleven temperatures. Expressly, the MQW-SOA temperature was varied using a Peltier element (PE) and a thermoelectric temperature controller (TTC) with ±0.2°C accuracy (see Fig. 1). The results are presented in Fig. 3, where the experimental data for $E_{x_{sc}}$, $E_{x_{oc_{1,2}}}$, and $V_{bt_{1,2}}$ are shown with their linear interpolations accompanied by their respective formulas.

Figure 4 shows the e_{14_e}, $\bar{A}_{ehh}$, and $\Delta E_{s_{sc}}$ values (open crosses) calculated as a function of temperature using Eqs. (3), (5)–(9) and the last term on the right-hand side (RHS) of Eq. (4) ($-\bar{A}_{ehh} L_w^4 F_{w_{sc}}^2$) together with the experimentally obtained values of $E_{x_{sc,oc_{1,2}}}$ and $V_{bt_{1,2}}$ reported in Fig. 3 (marks).

These parameters were also calculated using the linear interpolation formulas for $E_{x_{sc,oc_{1,2}}}$ and $V_{bt_{1,2}}$ given in Fig. 3, resulting in the values represented with open circles in Fig. 4. Moreover,

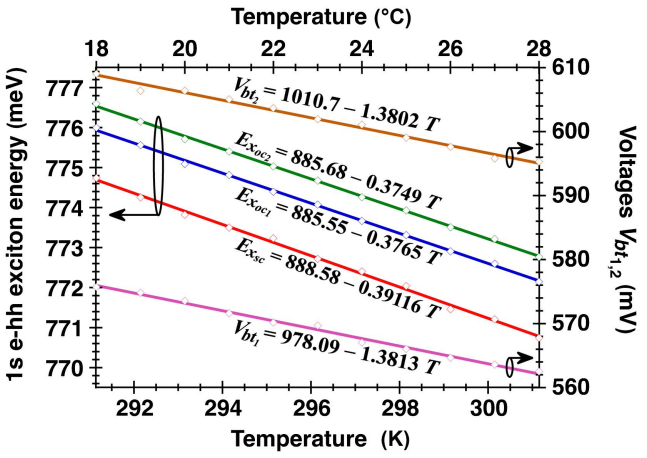

Fig. 3. $E_{x_{sc,oc_{1,2}}}$ and $V_{bt_{1,2}}$ versus temperature. Marks and traces are the measured values and their linear interpolations accompanied by their respective formulas.

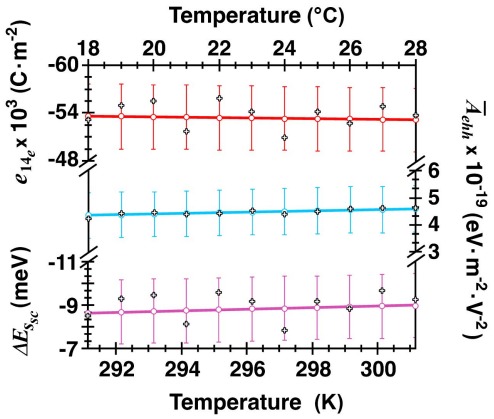

Fig. 4. e_{14e}, $\bar{A}_{ehh}$, and $\Delta E_{s_{sc}}$ versus temperature (upper, middle, and lower graphs) calculated using experimentally obtained values (open crosses) and interpolated values (open circles and their interpolations with solid lines) of $E_{x_{sc,oc_{1,2}}}$ and $V_{bt_{1,2}}$.

the precisions $\pm\Delta e_{14_e}$, $\pm\Delta\bar{A}_{ehh}$, and $\pm\Delta\Delta E_{s_{sc}}$ with which the e_{14_e}, $\bar{A}_{ehh}$, and $\Delta E_{s_{sc}}$ values were extracted from the experimental data are represented in the graphs of Fig. 4 with error bars and were obtained in a manner similar to that described in Ref. [11]. Due to the high absorption of the $1S_{e\text{-}hh}ER$, the OSA noise floor generates inaccuracies in the determination of $E_{x_{sc,oc_{1,2}}}$, which is the main cause of the dispersion of the e_{14_e}, $\bar{A}_{ehh}$, and $\Delta E_{s_{sc}}$ values represented with open crosses in Fig. 4. However, all these values, calculated directly with the experimental data reported in Fig. 3 (marks), do not exceed the limits of the error bars, which validates the precision wherewith e_{14_e}, $\bar{A}_{ehh}$, and $\Delta E_{s_{sc}}$ are estimated. In particular, the extracted e_{14_e} values at 18, 23, and 28°C are -0.0536 ± 0.0041, -0.0534 ± 0.0040, and -0.0531 ± 0.0040 C · m^{-2}, respectively, i.e., in the analyzed temperature range, the result accuracy is approximately equal to ± 0.004 C · m^{-2}, which is similar to that obtained by other methods extracting the e_{14_e} value[13]. Moreover, as expected, these e_{14_e} values, and in general all those reported in the upper graph of Fig. 4, evidence that the e_{14_e} magnitude tends to decrease as temperature increases. Indeed, as temperature rises, the electric dipole randomization increases. Hence, the strain-induced polarization decreases together with e_{14_e}.

It is relevant to mention that this behavior is contrary to that observed in other previously published work where the piezoelectric constant magnitude in $In_{1-x}Ga_xAs$ QWs increases as temperature increases, for which no convincing explanation has been presented[13–17]. To gain more insight into this contradictory aspect, we further investigate the behavior regarding the temperature of the $1S_{e\text{-}hh}ER$ total Stark shift under SCC ($\Delta E_{s_{sc}}$). As shown in the lower graph of Fig. 4, the $\Delta E_{s_{sc}}$ magnitude increases as the temperature increases. Vis-a-vis the behavior exhibited by e_{14_e}, the $\Delta E_{s_{sc}}$ behavior concerning temperature would seem to be opposite to that expected since the $\Delta E_{s_{sc}}$ magnitude is directly proportional to $F_{w_{sc}}^2$, which is in turn directly proportional to $e_{14_e}^2$ [see the last terms on the RHS of Eqs. (4) and

(2) with $V_{\mathrm{bt}_n} = 0$]. However, $\Delta E_{s_{sc}}$ also depends on the parameter $\bar{A}_{\mathrm{ehh}}$ whose magnitude increases as the temperature increases, as shown in the middle graph of Fig. 4. Although $\bar{A}_{\mathrm{ehh}}$ contributes linearly to the $\Delta E_{s_{sc}}$ magnitude, its growth rate with increasing temperature is strong enough to overcome the antagonistic rate of the quadratic contribution from e_{14_e}. For this reason, the $\Delta E_{s_{sc}}$ magnitude increases as temperature increases. The parameter $\bar{A}_{\mathrm{ehh}}$, which can be determined by performing indirect measurements and applying Eq. (6), is physically a function of the out-of-plane effective masses ($m^{\perp}_{w_{e,\mathrm{hh}}}$) and the ground state energy shift enhancement factors ($\Omega_{e,\mathrm{hh}}$), due to the finite value of the barrier height, of electrons and heavy holes[12]. Consequently, in models where $m^{\perp}_{w_{e,\mathrm{hh}}}$ and $\Omega_{e,\mathrm{hh}}$ are used explicitly instead of $\bar{A}_{\mathrm{ehh}}$, it becomes essential that these parameters are a function of temperature. Otherwise, the change that the $1S_{e\text{-}hh}ER$ total Stark shift would undergo with temperature would be solely attributed to e_{14_e}, and vice versa. If the Stark shift behavior were used to determine that of e_{14_e}, then an erroneous comportment of e_{14_e}, contrary to that found in this work, would be obtained. We speculate that the discrepancy between the piezoelectric constant behavior regarding temperature estimated in this work and that reported by other authors might be due to the omission of the temperature dependences of $m^{\perp}_{w_{e,\mathrm{hh}}}$ and electron (heavy hole) energy in the QWs, or an imprecise description of them, possibly because of the lack of detailed reports on these issues.

Finally, Fig. 2 shows that by varying the temperature from 18 to 28°C, the $1S_{e\text{-}hh}ER$ operation energy can be tuned 4 meV, and then, under OCC, fluctuating the input power from −15.9 to 5 dBm, this resonance can be shifted 3.7 meV, as shown in Fig. 5. It is important to note that if the input signal were composed of pulses whose duration was less than the escape time of the carriers in the QWs plus the time it takes them to drain through the circuit formed by parasitic elements and the amplifier electrodes, then, under SCC, the power of each input pulse would also shift $1S_{e\text{-}hh}ER$.

This opens the possibility of devising ultra-fast all-optical applications using unbiased MQW-SOAs since there would be no free carriers that would generate slow tails in the falling edges of the output pulses as might occur under OCC, notably with high input powers. A study of the Stark effect dynamics under SCC and OCC is currently in progress.

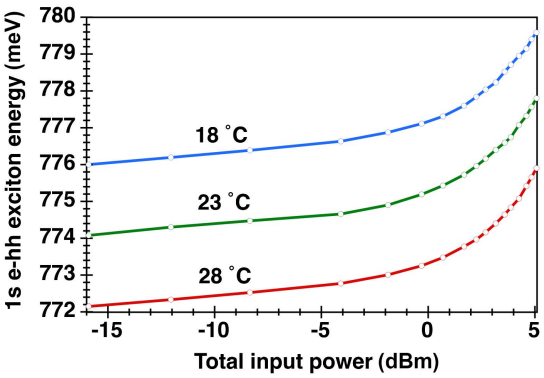

Fig. 5. $1S_{e\text{-}hh}ER$ energy versus total input power at 18, 23, and 28°C. Marks and traces are the measured values and their interpolations.

4. Conclusion

We presented a procedure for determining the effective piezoelectric constant value of the [111]-oriented strained $In_{1-x}Ga_xAs/In_{1-x}Ga_xAs_yP_{1-y}$ QWs of an MQW-SOA. Remarkably, the proposed method is insensitive to the temperature dependence of the bandgap energy and the segregation phenomenon. Likewise, it requires neither fitting parameters nor temperature-dependent expressions for energy and out-of-plane effective masses of electrons and heavy holes. When the procedure was applied to the MQW-SOA under study, a value of $e_{14_e} = -0.0534 \pm 0.0040\ \mathrm{C \cdot m^{-2}}$ at 23°C was obtained. Unlike previously published methods, where the piezoelectric constant magnitude increased as the temperature rised without convincing explanation, we extracted an e_{14_e} magnitude that decreased as temperature increased. Even though the method was specially designed for experimentally determining e_{14_e} in MQW-SOAs, it can be applied to any p-iMQW-n structure with electrodes and strained [111]-oriented zinc-blende QWs. Finally, we found that by varying temperature, the $1S_{e\text{-}hh}ER$ operation energy could be tuned, and then, fluctuating the input power, this resonance could be significantly shifted. This enables the devising all-optical applications based on QCSE in unbiased MQW-SOAs. Thus, for example, the method can be applied to other MQW-SOAs, intended to implement all-optical functions based on the QCSE, to predict the shift of their $1S_{e\text{-}hh}ER$ with temperature, or to indirectly deduce how temperature will affect the undesirable effects that QCSE causes in some MQW LEDs.

Acknowledgement

This work was partially supported by the Mexican Council of Science and Technology (CONACYT) (Nos. SEP-CONACYTCB-2016-01-285030 and 804835).

References

1. E. Baldini, A. Domínguez, T. Palmieri, O. Cannelli, A. R. Secades, P. Ruello, and M. Chergui, "Exciton control in a room temperature bulk semiconductor with coherent strain pulses," Sci. Adv. **5**, eaax2937 (2019).
2. H. Soto, M. A. Tong, J. C. Domínguez, and R. Muraoka, "Demonstration of an all-optical feed-forward delay line buffer using the quadratic Stark effect and two-photon absorption in an SOA," Opt. Express **25**, 22066 (2017).
3. H. Saidi, O. Zitouni, and S. Ridene, "Investigation of orientation dependence of piezoelectric effects in strained GaAs/InGaAs quantum well laser," Mater. Sci. Eng. B **273**, 115400 (2021).
4. H. Soto-Ortiz, G. Torres-Miranda, and R. Muraoka-Espíritu, "Study of the quantum-confined Stark effect in an unbiased [111]-oriented multi-quantum well semiconductor optical amplifier," Opt. Commun. **529**, 129081 (2023).

5. G. Bester, X. Wu, D. Vanderbilt, and A. Zunger, "Importance of second-order piezoelectric effects in zinc-blende semiconductors," Phys. Rev. Lett. **96**, 187602 (2006).
6. J. D. Bruno and R. L. Tober, "Effects of the piezoelectric field on quantum-confined Stark effect in (111)B InGaAs quantum-well structure," J. Appl. Phys. **85**, 2221 (1999).
7. S. Cho and A. Majerfeld, "Temperature dependence of excitonic properties of (111)B InGaAs/GaAs piezoelectric and pyroelectric multiquantum wells," J. Appl. Phys. **106**, 023527 (2009).
8. G. Gonzalez de la Cruz, A. Calderon Arenas, and H. Herrera, "Internal electric-field and segregation effects on luminescence properties of quantum wells," J. Appl. Phys. **98**, 023501 (2005).
9. M. Moran, H. Meidia, T. Fleischmann, D. J. Norris, G. J. Rees, A. G. Cullis, and M. Hopkinson, "Indium segregation in (111)B GaAs-$In_xGa_{1-x}As$ quantum wells determined by transmission electron microscopy," J. Phys. D **34**, 1943 (2001).
10. P. Ballet, P. Disseix, J. Leymarie, A. Vasson, A.-M. Vasson, and R. Grey, "The determination of e_{14} in (111)B-grown (In,Ga)As/GaAs strained layers," Thin Solid Films **336**, 354 (1998).
11. H. Soto-Ortiz and G. Torres-Miranda, "Direct determination of the piezoelectric field using the quantum-confined Stark effect in a strained [111]-oriented zinc-blende MQW-SOA," AIP Adv. **12**, 105005 (2022).
12. G. Bastard, E. E. Mendez, L. L. Chang, and L. Esaki, "Variational calculations on a quantum well in an electric field," Phys. Rev. B **28**, 3241 (1983).
13. J. J. Sánchez, J. I. Izpura, J. M. G. Tijero, E. Muñoz, S. Cho, and A. Majerfeld, "Confirmation of the pyroelectric coefficient of strained $In_xGa_{1-x}As$/GaAs quantum well structures grown on (111)B GaAs by differential photocurrent spectroscopy," J. Appl. Phys. **91**, 3002 (2002).
14. S. Cho, J. Kim, A. Sanz-Hervás, A. Majerfeld, G. Patriarche, and B. W. Kim, "Characterization of piezoelectric and pyroelectric properties of MOVPE-grown strained (111)A InGaAs/GaAs QW structures by modulation spectroscopy," Phys. Status Solidi A **195**, 260 (2003).
15. T. B. Bahder, R. L. Tober, and J. D. Bruno, "Temperature-dependent polarization in [111] $In_xGa_{1-x}As$-$Al_xGa_{1-x}As$ quantum wells," Phys. Rev. B **50**, 2731 (R) (1994).
16. S. Cho, A. Majerfeld, A. Sanz-Hervás, J. J. Sánchez, J. L. Sánchez-Rojas, and I. Izpura, "Determination of the pyroelectric coefficient in strained InGaAs/GaAs quantum wells grown on (111)B GaAs substrates," J. Appl. Phys. **90**, 915 (2001).
17. S. Cho, A. Majerfeld, J. J. Sánchez, E. Muñoz, J. M. G. Tijero, and J. I. Izpura, "Observation of the pyroelectric effect in strained piezoelectric InGaAs/GaAs quantum-wells grown on (111) GaAs substrates," Microelectron. J. **33**, 531 (2002).